Automated Levee Detection in Digital Elevation Models

M. Pronk [a,b], M. Gawehn [a], M. Eleveld [a,c], H. Ledoux [b]

[a] *Deltares, P.O. Box 177, 2600 MH, Delft, the Netherlands*
[b] *Urban Data Science, Architecture and the Built Environment, Delft University of Technology, Julianalaan 134, 2628 BL, Delft, the Netherlands*
[c] *Mathematical Geodesy and Positioning, Civil Engineering & Geosciences, Delft University of Technology, Stevinweg 1, 2628 CN, Delft, the Netherlands*

Abstract

Current flood risk models applied at national and global scales do not—or only partially—take levees into account, resulting in inaccurate flood inundation maps. While levees are important assets in natural hazard risk assessments, accurate information in the public domain about the location and height of these embankments is often missing. Remote sensing data—such as global digital elevation models (DEMs)—contain this information, in theory. However, their low resolution and vertical biases (caused by the canopy and infrastructure) complicate the extraction of levees. We present a new DEM processing method to identify and extract levees from any high-resolution DEM as continuous features, including related attributes such as the protected area and volume. As a test case, we use CopernicusDEM GLO-30 and local DEMs. Validation against reference data from the United States and the Netherlands yields a recall of up to 88 % on a local DEM and up to 51 % when applied to the 30 m resolution global DSM. The method also identifies other water-retaining barriers such as undocumented dams. Incorporating levees derived from these methods into flood risk models should enable practitioners to construct more accurate (coastal) flood inundation maps on national and global scales.

Keywords: embankment, levee, CopernicusDEM, mathematical morphology, terrain processing, flood risk

1. Introduction

Flood-protection levees (also called embankments or dikes) are crucial assets in flood risk assessments, as they can significantly influence flood extent and

depth. Indeed, flood inundation models—especially those with coarse grid resolutions that exceed the width of a levee—explicitly require structures such as levees to be included in the model (van Ormondt et al., 2025). However, accurate information in the public domain about the location, shape, and height (i.e., a 3D linestring of the crest) of these levees is often missing. As such, current flood risk models applied at national and global scales do not—or only partially—take levees into account, often resulting in inaccurate flood inundation maps.

There are national databases detailing levees, such as the National Levee Database (NLD) (USACE, 2024) from the US Army Corps of Engineers (USACE) in the United States. However, these databases are often incomplete, as they rely on local authorities to provide the information. In addition, the national databases are not internationally standardised, making it difficult to compare levees across countries.

Nienhuis et al. (2022) therefore made a global inventory of levees, unifying public (national) datasets. While this is a great step forward—and done in a FAIR (Wilkinson et al., 2016) manner—it showcases how incomplete the global coverage is, with many countries—especially in the Global South—having no data available. A more recent initiative is the Global Levee Database Inventory (GLDI) (Boulange et al., 2025). Other global but generic databases, such as OpenStreetMap, sometimes contain levees, but are not guaranteed to do so, and the labels are not standardised (Vargas-Munoz et al., 2021).

Given this knowledge gap, several studies have implemented (semi-)automated methods to find levees from data such as gridded DEMs. Steinfeld et al. (2013) compared three semi-automated segmentation and one visual interpretation method to find levees in the Gwydir floodplain in Australia. Czuba et al. (2015) reported a USGS pilot study to find undocumented levees in the US using local DEMs, identifying possible candidates using visual interpretation of a hillshade, and a semi-automated wavelet-based (edge detection) method, after which a field survey was conducted for validation. Wing et al. (2019)—recognizing the need for a fully automated method for coarser elevation models (10 m to 30 m)—developed a model to identify DEM cells that are likely to be levees based on geomorphic features (e.g., slope, curvature), calibrated on the NLD. These cell-candidates are then used as the representative elevation, instead of an aggregate (mean, median), for a coarser flood inundation model. Likewise, Khanh et al. (2025) extract levees from 10 m resolution DEMs in five countries based on geomorphic features. Van Nieuwenhuizen et al. (2021) automatically identify and remove (infrastructure) embankments from fine-resolution DEMs (e.g., a 1 m resolution) by region growing from a given road or rail network based on the shape (slope)

of the embankment. Knox et al. (2022a) use several machine learning methods to identify potential levees in the US based on geomorphic, hydraulic, and land cover features, and—like Nienhuis et al. (2022)—published the results as an open dataset (Knox et al., 2022b). All the above studies apply their methods to individual cells, and results are thus prone to having gaps (cell misclassification) in the levees, thereby nullifying the purpose of the levee as a continuous flood barrier.

In this paper, we present a new terrain processing method to identify and extract potential levees as continuous features (objects) from any high-resolution DEM. Our approach builds on Wood et al. (2018), who used radar-based flood extent maps and combined them with local gauge information to detect levees. If the gauge showed a large range of water levels, while the flood extent stayed the same, a levee was likely to be present. This method is somewhat similar to how practitioners would visually recognise leveed areas (and thus levees) in an elevation (contour) map (Ehlschlaeger, 1989).

We apply our generic method to the CopernicusDEM GLO-30 dataset (European Space Agency and Airbus, 2022) and local elevation models to identify levees, and validate the results with reference data from the United States and the Netherlands. Flood risk models that incorporate levees derived from these methods should enable more accurate (coastal) flood inundation maps on national and global scales.

2. Material and methods

2.1. Concepts and method

Following the train of thought of visual recognition—translating flood extents as leveed areas into an algorithm—we can artificially inundate the DEM at discrete, increasing water levels. Astute readers will recognise that this procedure is similar to (earlier) depression filling or watershed delineation algorithms, such as those of Beucher and Meyer (1992) and Bleau and Leon (2000). We therefore note that (artificial) flood extents outline *depressions* in the landscape; these depressions can be created by barriers such as levees (Insight 1), with the *spill point* being the lowest point on the levee crest. Potential leveed areas (and therefore levees) can thus be identified by finding depressions in the DEM (Implication 1).

Insight 1. *The area protected by a levee forms a depression in the landscape, with the spill point as the lowest point of the levee crest.*

Implication 1. *Leveed areas (and thus the levee) can be found by identifying depressions in a digital elevation model.*

Insight 2. *The levee crest is part of the watershed boundary, with the spill point of the depression as the watershed outlet.*

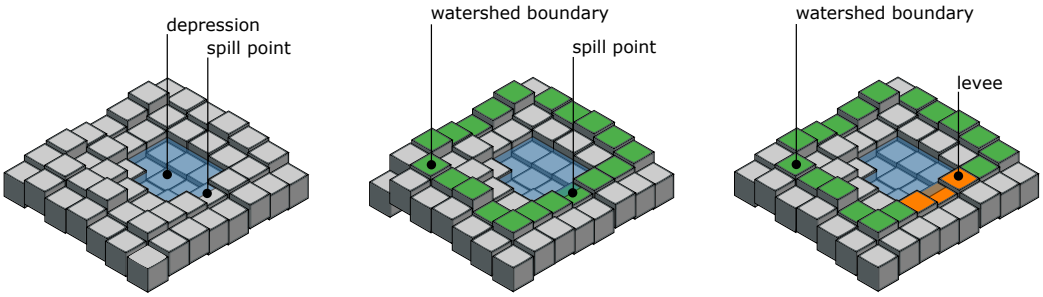

Figure 1: A schematisation of the method. Given an elevation model—represented as elevation cells here—a modified Priority-Flood algorithm is used to identify depressions and their spill points. From there, the watershed boundary with the spill point as its outlet is determined, of which the levee is part of.

Given a depression with a levee, the levee crest is part of the watershed boundary with the spill point as the outlet of the watershed (Insight 2). This is illustrated spatially in Figure 1.

These potential levee crests (watershed boundaries) resulting from this method are circular and range from small ponds to large valleys. While (nested) circular (ring) levees exist—most notably in polder systems—most levees are non-circular features, and we thus need to reduce the watershed boundary to the actual levee crest. In addition, filtering is required to exclude natural depressions in the landscape (e.g., salt flats) that are not leveed areas.

By analysing groups of cells (e.g., a depression or watershed) instead of individual cells, we can identify levees as continuous features. This also allows us to derive related attributes, such as depression volume, average depth, and perimeter length, that are unavailable to cell-based methods. These attributes can then be used to filter the potential levees based on local knowledge (e.g., minimum leveed area size).

We adapted the Priority-Flood algorithm (Barnes et al., 2014) to efficiently compute depressions, flow directions, and related attributes in the same pass. Inspired by the earlier work of Wu et al. (2019), we further adapted the Priority-Flood algorithm to compute *nested* depressions, as levees can be nested (e.g., in polder systems). The pseudo-code is given in Supplementary Material 1. The final algorithm classifies DEM cells as potential levees for each depression in the DEM, while tracking group attributes. For distribution, we vectorise the classified

levee cells, and save the resulting linestrings with their attributes in the GeoPackage file format. We have written the above procedures in the Julia programming language (Bezanson et al., 2017), using the Geomorphometry.jl (Pronk, 2026b) and Rasters.jl packages, and have made it available as an open-source (GPL 3.0 licensed) package on GitHub (`https://github.com/evetion/Breach.jl`) (Pronk, 2026a). The repository also contains the dataset samples presented in this paper.

2.2. Datasets

Elevation data

We apply our method to airborne lidar-derived digital elevation models in two test areas with a high levee density: the Mississippi River Delta in the US (where the term levee originated (Winsor, 1895)) and the Netherlands (where there are 22 000 km of levees). For the US, we use the National Elevation Database (NED) (United States Geological Survey, 2021) at 10 m resolution—distributed via OpenTopography—while for the Netherlands we use the national Dutch Elevation Model (AHN4, Het Waterschapshuis (2022)) at 5 m resolution. Given the need for a global levee dataset, we also apply our method to the latest global DEM, specifically the CopernicusDEM GLO-30 dataset for the same areas, provided under COPERNICUS by the European Union and ESA (European Space Agency and Airbus, 2022). The dataset is distributed in tiles of 1 degree by 1 degree, with a spatial resolution of one arcsecond (~30 m at the equator).

Reference data

To validate the method, detected levees are compared with reference data from the United States and the Netherlands. Specifically, we rasterise the linestrings from the Alignment Lines layer from the National Levee Database (NLD) (USACE, 2024) for the US and the current levees from the cultural heritage levee dataset (RCE dijkenkaart) (Rijksdienst voor het Cultureel Erfgoed, 2021) of the Netherlands, onto the DEMs. We rasterise lines to all cells they touch (single-cell width) and assume that they represent the levee crest.

2.3. Metrics

To investigate the performance of our method, we compute levees in two different areas (in the US and the Netherlands as mentioned above), with different DEM sources (global and local) and resolutions (10 m to 15 m and 30 m). Higher resolutions (e.g., 5 m) also work well with the method, but are not used here due to the computational cost at the scale of the validation areas.

Because custom filtering is required to (a) exclude natural depressions, and (b) find the part of the circular watershed boundary that is levee (see Figure 1), we compute three variants: (1) the full watershed boundary without filters (full variant) as a baseline, (2) these watersheds filtered on a minimum depression volume of 50 000 m^3 (filtered variant, to account for a), and (3) the part of the filtered watershed boundaries vertically within 3 m of the spill point height (partial variant, to account for a and b). For each combination, we compare the detected levees with the rasterised reference data using confusion matrix metrics: precision, recall, and F_1 score (Fawcett, 2006). Note that we do not report true negative rate (related) metrics, as the number of real negatives (all cells without levees) far exceeds the number of levee cells.

3. Results

3.1. Validation

When applied to the validation areas in the US and the Netherlands, our method is able to identify the majority of levees, even when applied to the 30 m DSM (Table 1). A spatial subset (an area that was subject to a major storm surge in 1953, which led to the Dutch Delta Works (Deltacommissie, 1954)) of the results for the Netherlands is shown in Figure 2, while a subset for the US is provided as Supplementary Material 2. Going from a 30 m DSM to a 15 m DTM for the full variant increases the recall from 50% to 62% in the Netherlands, and from 37% to 80% in the US. The metrics for the 30 m DTM are slightly better than the 15 m or 10 m DTM in both the Netherlands (0.68 and 0.62 recall for the full variant) and the US (0.88 and 0.80 recall for the full variant).

Applying a minimum volume filter of 50 000 m^3 (filtered variant) increases the overall precision (0.05 to 0.11 for the NL 30 m DTM) and F_1 score slightly (0.10 to 0.18 for the NL 30 m DTM), but at the cost of recall (0.88 to 0.77 for the US 30 m DTM). Filtering out the levee from the watershed boundary using a vertical 3 m tolerance around the spill point (partial variant) decreases all metrics, and decreases precision considerably (0.57 to 0.40 for the NL 15 m DTM), indicating an increase in false negatives.

The precision and F_1 score are low across datasets and variants, indicating many false positives. Indeed—especially in the DSM (see Figure 2)—many depressions in the landscape are detected as leveed areas.

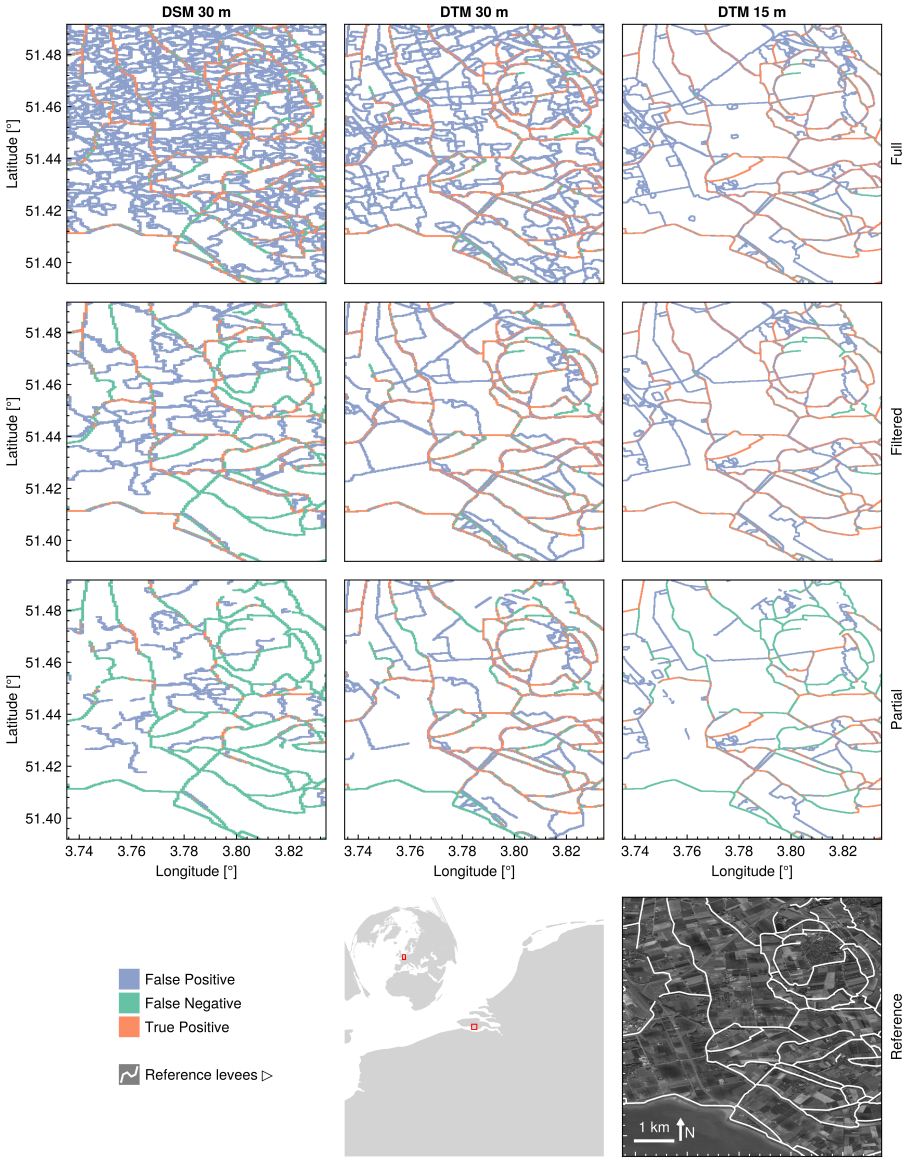

Figure 2: Validation of the levee detection method—using the full (complete watershed) results—in an example area around Zuid-Beveland in the Netherlands using (a) CopernicusDEM GLO-30 DSM, (b) airborne lidar-derived DTM at 30 m resolution, and (c) airborne lidar-derived DTM at 15 m resolution. The light blue cells are the detected levees (false positive), while the green cells are the reference data (false negative). The orange cells are the intersection of the two (true positive). Even at a 30 m resolution DSM, half of the levees are correctly identified, with higher precision at higher resolution DTMs.

				Full			Filtered			Partial		
Area	Res	Src	N	P	R	F_1	P	R	F_1	P	R	F_1
NL	30 m	DSM	525 757	0.02	0.51	0.04	0.03	0.28	0.05	0.03	0.06	0.04
NL	30 m	DTM	525 757	0.05	0.68	0.10	0.11	0.56	0.18	0.11	0.40	0.17
NL	15 m*	DTM	1 379 283	0.08	0.62	0.12	0.09	0.57	0.16	0.09	0.40	0.15
US	30 m	DSM	120 450	0.0	0.37	0.01	0.0	0.25	0.02	0.01	0.07	0.01
US	30 m	DTM	120 450	0.01	0.88	0.03	0.04	0.77	0.08	0.02	0.33	0.04
US	10 m*	DTM	362 035	0.01	0.80	0.02	0.06	0.71	0.12	0.03	0.16	0.04

Table 1: Validation statistics for the Netherlands (NL) and the Mississippi River Delta (US), for both local airborne lidar DTMs (30 and 10 m resolution (Res)) and the global CopernicusDEM DSM (30 m). The number of true levee cells (N) is given, and precision (P), recall (R), and F_1 are reported for three levels of filtering: full (complete circular watershed boundary), filtered (watershed boundary with a minimum depression volume of 50 000 m^3), and partial (filtered watershed vertically within 3 m of the spill point height). * We allow cells within 1 cell of the reference data to be classified as true positives as well, to account for the geolocation uncertainty of the reference data.

4. Discussion

4.1. Filtering

The high recall of the full variants across different DEMs demonstrates the validity of our approach to identify levees from depressions in the landscape. Furthermore, the filtered variant shows the potential of using derived feature attributes unique to the method (such as depression volume) to filter out false positives. However, the partial variant filter is not sufficient to identify the levee crest, as many levees have a higher elevation difference between the spill point and the rest of the levee crest. More traditional filters based on geomorphic features (e.g., slope, curvature, as used in (Wing et al., 2019; Khanh et al., 2025; Knox et al., 2022a)) could be applied to derive the levee crest instead, with the added benefit of only needing to be computed for the watershed boundary instead of the full DEM. Users can filter potential levees—using the GeoPackage output interactively in a GIS or programmatically—based on their local knowledge, or from additional data sources, such as satellite imagery. Nonetheless, like Knox et al. (2022a), we would also argue that the reference datasets are incomplete (especially the case of the NLD), and that many of our false positives are in fact real levees that are not in the reference data (also see section 4.3).

4.2. Limitations

The quality and composition of the elevation and reference data imposes limitations on the accuracy of the method. For example, when applied to a global elevation model such as CopernicusDEM that represents the surface of the Earth (and not the bare Earth, thus including vegetation and buildings), it cannot detect levees that are covered by vegetation, and the method is prone to misclassifying urban or vegetation-covered areas as levees. Likewise, because a DEM provides only a 2.5D representation, non-water-retaining structures—such as bridges or embankments with culverts—may be incorrectly classified as levees. While the rasterisation of the reference (linestring) data makes a comparison possible, it introduces new biases (Fisher, 1997) depending on the rasterisation method and resolution. Indeed, Figure 2 shows false positive and negative cells neighbouring the reference data, indicating the results can be better in practice than the metrics suggest.

Finally, the method assumes that water levels are perfectly horizontal, which is not the case in reality. Especially for levees along large stretches of river, the river slope can cause misidentification of levees due to the spill point being too far downstream (i.e., at the lowest elevation instead of at the lowest height above the water surface). Future work could investigate using normalised or relative elevation models, such as height above the nearest drainage (HAND) (Nobre et al., 2011), to account for this.

4.3. Other applications

When applied in test areas around the globe (without reference datasets), we notice that our method is not limited to levees, but can also identify other water-retaining barriers (whether they keep water in or out) such as infrastructure embankments (e.g., highways, railways) and dams. For example, we were able to identify two dams that recently collapsed, causing catastrophic flooding in Libya in September 2023 (Figure 3a) and Sudan in August 2024 (Figure 3b), respectively. These dams are not present in the Global Dam Watch (GDW) dataset (Lehner et al., 2024), but were identified by our method, presumably because these dams do not normally impound a (permanent) reservoir and are thus difficult to detect from satellite imagery.

Author contributions

M. Pronk: Conceptualization, Investigation, Methodology, Software, Writing–Original Draft. M. Gawehn: Investigation, Writing–Reviewing and Editing. M.

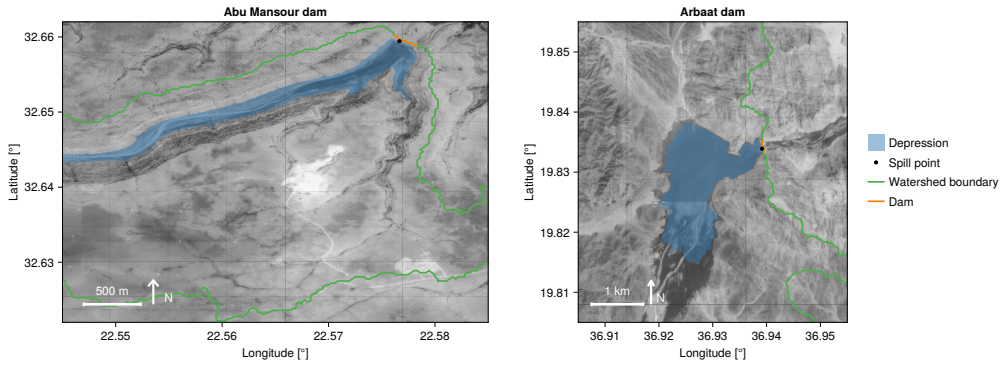

(a) (b)

Figure 3: Identification of several earthen dams: (a) the Abu Mansour dam in Libya, which collapsed on 10 September 2023, (b) the Arbaat dam in Sudan, which collapsed on 24 August 2024. Both were not present in the Global Dam Watch database (Lehner et al., 2024). The depression is the blue polygon, the watershed is the green line, whereas the dam is an orange line. The spill point is marked as a dot, and the background is greyscale Google Maps satellite imagery (©2025 Google).

Eleveld: Writing–Reviewing and Editing, Supervision. H. Ledoux: Writing–Reviewing and Editing, Supervision.

Funding

This research did not receive any specific grant from funding agencies in the public, commercial, or not-for-profit sectors.

Appendix A. Supplementary material 1

We provide the pseudo-code of the adapted Priority-Flood algorithm in Algorithm 1. The Julia code is available in the GitHub repository (`https://github.com/evetion/Breach.jl`) (Pronk, 2026a).

Appendix B. Supplementary material 2

A spatial subset of the results for the US around New Orleans is shown in Figure B.4.

Algorithm 1 Adapted Improved Priority-Flood: This algorithm adapts the Improved Priority-Flood algorithm (Barnes et al., 2014, Algorithm 2) to identify nested depressions and their spill points, and track group attributes in the same pass. It does so by converting the *Pit* plain queue in the original to a *PriorityQueue*, and using it for each depression. The use of a priority queue guarantees a descent into the depression, and any descent from a previous ascending cell is a new (nested) depression. Comments indicate changes from the original.

Require: DEM
Let $Open$ be a priority queue
Let *Pit* be a priority queue ▷
Let $Closed$ have the same dimensions as DEM
Let $Closed$ be initialized to $false$
Let $Labels$ have the same dimensions as DEM ▷
Let $Labels$ be initialized to 0 ▷
Let *Breach* have the same dimensions as DEM ▷
Let *Breach* be initialized to $false$ ▷
label ← 0
for all c on the edges of DEM **do**
    Push c onto Open with priority DEM(c)
    Closed(c) ← true
end for
while either $Open$ or *Pit* is not empty **do**
    if Pit is not empty **then**
        c ← pop(Pit)
    else
        c ← pop(Open)
    end if
    for all neighbors n of c **do**
        if Closed(n) **then repeat loop**
        end if
        Closed(n) ← true

```
24:         if DEM(n) ≤ DEM(c) then
25:             if Labels(c) = 0 ∧ ¬ Breach(c) then          ▷ Begin of modification
26:                 register(label)        ▷ Stores minimum, parent and spill height
27:                 Breach(c) ← true
28:                 Labels(n) ← label
29:                 label += 1
30:             else if Breach(c) then
31:                 Labels(n) ← label − 1
32:             else
33:                 if (DEM(c) > minimum[Labels(c)]) ∧ (DEM(n) < DEM(c))
  then
34:                     register(label)   ▷ Stores minimum, parent and spill height
35:                     Breach(c) ← true
36:                     Labels(n) ← label
37:                     label += 1
38:                 else if DEM(n) < DEM(c) then
39:                     Labels(n) ← Labels(c)
40:                 else if DEM(n) ≥ spillheight[Labels(c)] then
41:                     Labels(n) ← parent[Labels(c)]
42:                 else
43:                     Labels(n) ← Labels(c)
44:                 end if
45:             end if                                       ▷ End of modification
46:             DEM(n) ← DEM(c)
47:             Push n onto Pit
48:         else
49:             Push n onto Open with priority DEM (n)
50:         end if
51:     end for
52:     update(label)                    ▷ Updates minimum with current cell
53: end while
54: finalize(labels)                     ▷ Propagate minimum to parent cells
```

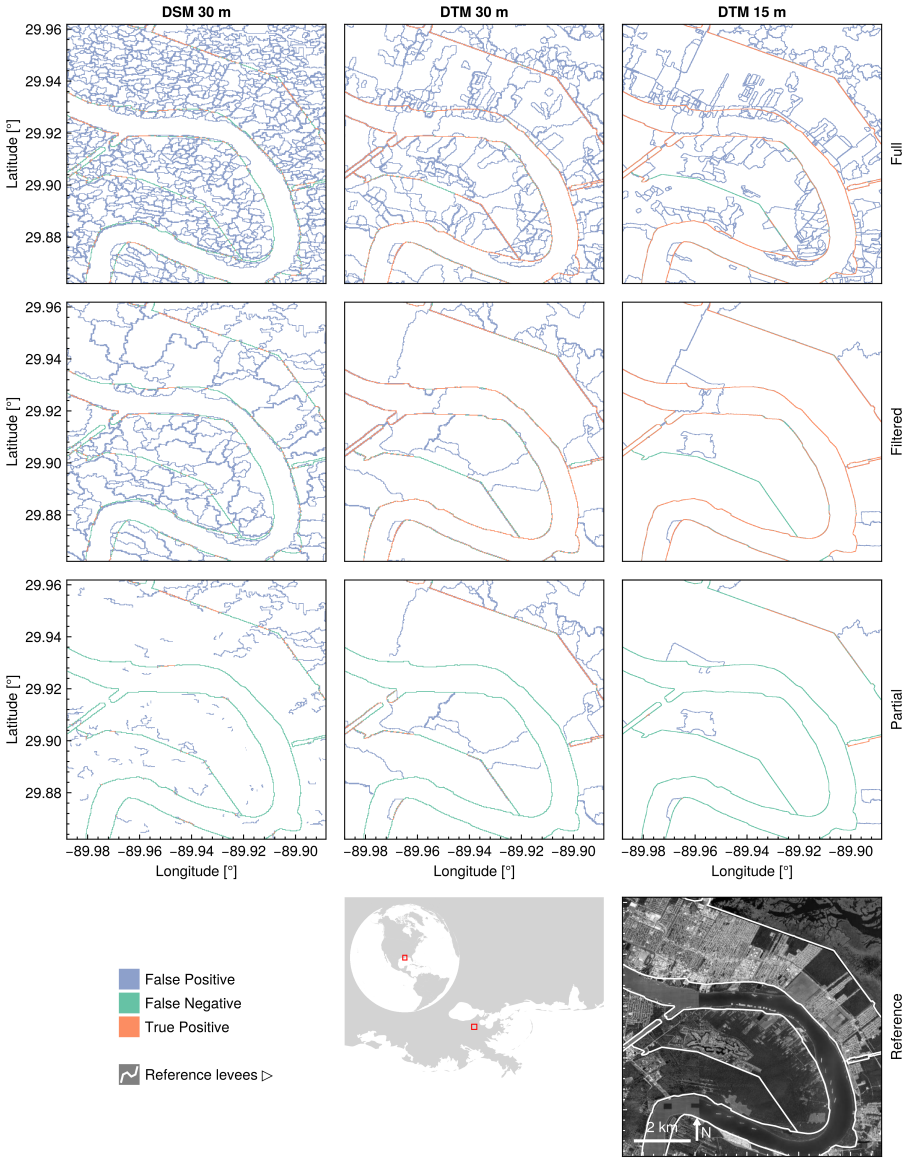

Figure B.4: Validation of the levee detection method—using the full (complete watershed) results—in an example area in New Orleans in the United States using (a) CopernicusDEM GLO-30 DSM, (b) airborne lidar-derived DTM at 30 m resolution, and (c) airborne lidar-derived DTM at 15 m resolution. The light blue cells are the detected levees (false positive), while the green cells are the reference data (false negative). The orange cells are the intersection of the two (true positive).

References

Barnes, R., Lehman, C., Mulla, D., 2014. Priority-Flood: An Optimal Depression-Filling and Watershed-Labeling Algorithm for Digital Elevation Models. Computers & Geosciences 62, 117–127. doi:10.1016/j.cageo.2013.04.024, arXiv:1511.04463.

Beucher, S., Meyer, F., 1992. The Morphological Approach to Segmentation: The Watershed Transformation, in: Mathematical Morphology in Image Processing. CRC Press.

Bezanson, J., Edelman, A., Karpinski, S., Shah, V.B., 2017. Julia: A Fresh Approach to Numerical Computing. SIAM Rev. 59, 65–98. doi:10/f9wkpj.

Bleau, A., Leon, L.J., 2000. Watershed-Based Segmentation and Region Merging. Computer Vision and Image Understanding 77, 317–370. doi:10.1006/cviu.1999.0822.

Boulange, J., Hirabayashi, Y., Rimba, A.B., Modi, P., 2025. A new generation of global flood protection database. International Journal of Disaster Risk Reduction 130, 105823. doi:10.1016/j.ijdrr.2025.105823.

Czuba, C., Williams, B., Westman, J., LeClaire, K., 2015. An Assessment of Two Methods for Identifying Undocumented Levees Using Remotedly Sensed Data. Technical Report 2015–5009. US Department of the Interior, US Geological Survey.

Deltacommissie, 1954. Afdamming zeearmen : derde interim-advies uitgebracht aan de minister van Verkeer en Waterstaat. Technical Report. Staatsdrukkerij- en Uitgeverijbedrijf. doi:10/afdamming-zeearmen-derde-interim-advies/.

Ehlschlaeger, C., 1989. Using the AT search algorithm to develop hydrologic models from digital elevation data, in: Proceedings of the International Geographic Information System (IGIS) Symposium, Baltimore, MD. pp. 275–281.

European Space Agency, Airbus, 2022. Copernicus DEM. doi:10.5270/ESA-c5d3d65. [dataset].

Fawcett, T., 2006. An introduction to ROC analysis. Pattern Recognition Letters 27, 861–874. doi:10.1016/j.patrec.2005.10.010.

Fisher, P., 1997. The pixel: A snare and a delusion. Int. J. Remote Sens. 18, 679–685. doi:10/bjgvkz.

Het Waterschapshuis, 2022. AHN4. doi:https://www.arcgis.com/home/item.html?id=77da2e9eeea8427aab2ac83b79097b1a. [dataset].

Khanh, D.N., Tsumura, Y., Sasaki, O., Shiraishi, K., Akimoto, D., Yamazaki, D., Zhao, G., Hirabayashi, Y., 2025. Mapping the World's River Levees: A Hyper-Resolution Levee Database Based on Digital Elevation Models. Geophys. Res. Lett. 52, e2024GL114121. doi:10.1029/2024GL114121.

Knox, R.L., Morrison, R.R., Wohl, E.E., 2022a. Identification of Artificial Levees in the Contiguous United States. Water Resour. Res. 58, e2021WR031308. doi:10.1029/2021WR031308.

Knox, R.L., Morrison, R.R., Wohl, E.E., 2022b. Potential levees. doi:10.4211/hs.729c0aea00bb48d6b6814c147e4318c4. [dataset].

Lehner, B., Beames, P., Mulligan, M., Zarfl, C., De Felice, L., van Soesbergen, A., Thieme, M., Garcia de Leaniz, C., Anand, M., Belletti, B., Brauman, K.A., Januchowski-Hartley, S.R., Lyon, K., Mandle, L., Mazany-Wright, N., Messager, M.L., Pavelsky, T., Pekel, J.F., Wang, J., Wen, Q., Wishart, M., Xing, T., Yang, X., Higgins, J., 2024. The Global Dam Watch database of river barrier and reservoir information for large-scale applications. Sci Data 11, 1069. doi:10.1038/s41597-024-03752-9.

Nienhuis, J.H., Cox, J.R., O'Dell, J., Edmonds, D.A., Scussolini, P., 2022. A global open-source database of flood-protection levees on river deltas (openDELvE). Nat. Hazards Earth Syst. Sci. 22, 4087–4101. doi:10.5194/nhess-22-4087-2022.

Nobre, A.D., Cuartas, L.A., Hodnett, M., Rennó, C.D., Rodrigues, G., Silveira, A., Waterloo, M., Saleska, S., 2011. Height Above the Nearest Drainage – a hydrologically relevant new terrain model. Journal of Hydrology 404, 13–29. doi:10/bs5wdq.

Pronk, M., 2026a. Evetion/Breach.jl. Zenodo. URL: https://zenodo.org/records/18850537, doi:10.5281/zenodo.18850537. [software].

Pronk, M., 2026b. Geomorphometry.jl. Zenodo. doi:10.5281/zenodo.18851929. [software].

Rijksdienst voor het Cultureel Erfgoed, 2021. RCE dijkenkaart. URL: https://www.nationaalgeoregister.nl/geonetwork/srv/api/records/c46f802d-929e-4c59-b53f-0f74b14724e4?language=all. [dataset].

Steinfeld, C.M.M., Kingsford, R.T., Laffan, S.W., 2013. Semi-automated GIS techniques for detecting floodplain earthworks. Hydrol. Process. 27, 579–591. doi:10.1002/hyp.9244.

United States Geological Survey, 2021. United States Geological Survey 3D Elevation Program 1/3 arc-second Digital Elevation Model. Distributed by OpenTopography. doi:10.5069/G98K778D. [dataset].

USACE, 2024. National Levee Database. URL: https://levees.sec.usace.army.mil/. [dataset].

Van Nieuwenhuizen, N., Lindsay, J.B., DeVries, B., 2021. Automated Mapping of Transportation Embankments in Fine-Resolution LiDAR DEMs. Remote Sens. 13, 1308. doi:10.3390/rs13071308.

van Ormondt, M., Leijnse, T., de Goede, R., Nederhoff, K., van Dongeren, A., 2025. Subgrid corrections for the linear inertial equations of a compound flood model – a case study using SFINCS 2.1.1 Dollerup release. Geosci. Model Dev. 18, 843–861. doi:10.5194/gmd-18-843-2025.

Vargas-Munoz, J.E., Srivastava, S., Tuia, D., Falcão, A.X., 2021. OpenStreetMap: Challenges and Opportunities in Machine Learning and Remote Sensing. IEEE Geosci. Remote Sens. Mag. 9, 184–199. doi:10.1109/MGRS.2020.2994107.

Wilkinson, M.D., Dumontier, M., Aalbersberg, I.J., Appleton, G., Axton, M., Baak, A., Blomberg, N., Boiten, J.W., da Silva Santos, L.B., Bourne, P.E., Bouwman, J., Brookes, A.J., Clark, T., Crosas, M., Dillo, I., Dumon, O., Edmunds, S., Evelo, C.T., Finkers, R., Gonzalez-Beltran, A., Gray, A.J.G., Groth, P., Goble, C., Grethe, J.S., Heringa, J., 't Hoen, P.A.C., Hooft, R., Kuhn, T., Kok, R., Kok, J., Lusher, S.J., Martone, M.E., Mons, A., Packer, A.L., Persson, B., Rocca-Serra, P., Roos, M., van Schaik, R., Sansone, S.A., Schultes, E., Sengstag, T., Slater, T., Strawn, G., Swertz, M.A., Thompson, M., van der Lei, J., van Mulligen, E., Velterop, J., Waagmeester, A., Wittenburg, P., Wolstencroft, K., Zhao, J., Mons, B., 2016. The FAIR Guiding Principles for scientific data management and stewardship. Sci Data 3, 160018. doi:10.1038/sdata.2016.18.

Wing, O.E.J., Bates, P.D., Neal, J.C., Sampson, C.C., Smith, A.M., Quinn, N., Shustikova, I., Domeneghetti, A., Gilles, D.W., Goska, R., Krajewski, W.F., 2019. A New Automated Method for Improved Flood Defense Representation in Large-Scale Hydraulic Models. Water Resour. Res. 55, 11007–11034. doi:10.1029/2019WR025957.

Winsor, J., 1895. The Mississippi Basin...: The Struggle in America Between England and France 1697-1763. Houghton Mifflin.

Wood, M., De Jong, S., Straatsma, M., 2018. Locating flood embankments using SAR time series: A proof of concept. Int. J. Appl. Earth Obs. Geoinformation 70, 72–83. doi:10.1016/j.jag.2018.04.003.

Wu, Q., Lane, C.R., Wang, L., Vanderhoof, M.K., Christensen, J.R., Liu, H., 2019. Efficient Delineation of Nested Depression Hierarchy in Digital Elevation Models for Hydrological Analysis Using Level-Set Method. JAWRA J. Am. Water Resour. Assoc. 55, 354–368. doi:10.1111/1752-1688.12689.